Mechanical and Microstructural Behavior of Dissimilar AA2014-T6 and AA7075-T6 Aluminium Alloys Joined by Friction Stir Welding

Mohammad Adil and Jyoti Mukhopadhyay

Abstract

The present work aims to investigate the mechanical and microstructural properties of dissimilar welding of 2014-T6 and 7075-T6 aluminium alloys of 6 mm thick sheets, using butt welded friction stir welding. The two distinct materials welded with the perpendicular to the rolling direction of the dissimilar weld zone. The welded joint was tested in tension at room temperature to investigate the mechanical response and also to observe the differences with the parent materials. The diversity in the properties across the weld and its material mixing behavior have considered by resolving the thermal cycle, hardness test, and microstructural analysis. Plastic deformation along with recrystallization during the welding process resulted in the formation of distinct zones which could be identified by their respective microstructures. SEM/EDS analysis was carried out to analysis the precipitates, which influenced the properties of the joints. Based on the present study, 840 rpm with 30 mm/min weld speed seemed to be optimum.

M. Adil
Department of Mechanical Engineering, Indian Institute of Technology Gandhinagar, Gandhinagar, 382355, Gujarat, India
e-mail: adil.mohammad@iitgn.ac.in

J. Mukhopadhyay (✉)
Department of Material Science & Engineering, Indian Institute of Technology Gandhinagar, Gandhinagar, 382355, Gujarat, India
e-mail: jm@iitgn.ac.in

Introduction

Friction stir welding (FSW) is a solid-state joining technique, was innovated in the United Kingdom at the welding institute 1991; such technology has widely been examined primarily for low melting point materials, i.e., Al, Cu, and Mg alloys [1]. From the initiation, it can be effectively joined or fabricated by using this process [2]. The process has established a broad range of applications such as automobile, marine, and aerospace sectors. Various research organizations are actively involved in this procedure [3]. Using the FSW process, the different properties of Al alloys can be accepted, which applied for making structural parts that have good structural strength [4]. The importance of the FSW process is to avoid material loss, thermal distortion, embrittlement, and residual stresses. The process is slow as compared to the conventional welding methods because, in the FSW process, the maximum temperature of the base metal is always lower than 80% [5]. The temperature generated in the Nugget zone is in the range of 0.6–0.95 Tm. FSW can likely replace the resistance spot welding and riveting of Al sheets in the automotive and aircraft industries, respectively [6]. Furthermore, no exceptional preparation of the specimens has required during the welding process. FS welding of Al alloys suggested high mechanical properties and low heat input compared with conventional welding techniques [7]. Conventional welding shows a dendritic structure in the fusion zone, which results in an extreme decrease in the mechanical properties [8]. As the FS Welding process is a solid-state technique in which solidification structure is absent in the weld and the issues related to the presence of brittle inter-dendritic and eutectic phases are vanished [9]. FSW is considered a green technology process; therefore, the process is energy efficient and minimize the distortion. It also neither requires shielding gas nor filler metals [10]. FSW can join the alloys of similar and dissimilar materials (i.e., Aluminium and Magnesium) having thickness limits from 50 to 0.5 mm plates [11] since it

provides predominantly mechanical properties in the weld zone.

The salient purpose of this research work is to examine the mechanical and microstructural evolution of two dissimilar welding alloys, i.e., AA2014 and AA7075 of having a butt joint thickness of 6 mm using FS Welding process. Brief objectives of this research are listed below:

- To evaluate the optimal parameters (i.e., welding speed, tool rotation speed and hardness of alloys) in FSW by joining dissimilar welding Al alloys.
- To recognize the variation of temperature at different tool rotational speeds.
- To study the mechanical properties (i.e., hardness and tensile strength) of the dissimilar welded zone.
- To investigate the material flow behavior of the welding zone.
- To examine the various microstructural aspects and compare the grain size of different welding zone while varying the tool rotation speeds.

Experimental Procedure

Selection of Materials

The high strength aluminum alloys can be widely used in the automobile and aerospace industries. It is also required to fabricate them to enhance their downstream applications. Accordingly, rolled sheets of these two alloys were procured from Nextgen steel and alloys from Mumbai for the present investigation. The sheets were cut in the following size (50 × 150 × 6) mm for the welding. The chemical composition of these alloys is shown in Table 1. The parameters considered concerning the study and their ranges are shown in Table 2.

Both 2XXX and 7XXX series are heat treatable Al-based alloys. These alloys have high stretch forming compatibility and excellent formability which are mostly used in aerospace and few in automotive applications are shown in Table 3.

Tool Materials and Its Features

The tool materials used should have excellent properties such as high strength, good creep resistance, and good compressive yield strength. Colligan et al. [12] have reported the movement of material flow by the tool having a thread that helped to deliver the severe deformation of plasticization around the probe in FS Welding. Therefore, the tool selection depends upon several factors, such as the strength of workpiece, hardness, elevated temperature, etc.

Recent studies observed that the H13 steel tool (Fig. 1) was most preferred for the FSW process in softer materials. The tool consisted of the pin, which comes in contact with the workpiece and then plunged in the weld region. The FS shoulder of the tool inhibited the material from escaping the plasticized material during the FSW. Accordingly, the tool should have the cylindrical threaded pin profile, which as given in Table 4.

Table 1 Chemical configuration of AA2014-T6 and AA7075-T6 Al alloys

Alloys designation	Contents of alloying elements (%)								
	Cu	Mg	Mn	Si	Cr	Zn	Fe	Ti	Al
AA2014-T6	4.2	0.45	0.59	0.592	0.02	0.21	0.19	0.021	93.75
AA7075-T6	1.29	2.41	0.18	0.25	0.219	5.29	0.21	0.05	90.01

Table 2 Process parameters along with domain

S. No.	Parameters	Unit	Ranges				
1	Tool rotational speed	Rpm	540	660	840	1020	1200
2	Welding speed	mm/min	30				
3	Tool shoulder dia. to pin dia. ratio	–	=(20/6) 3.333				

Table 3 Mechanical properties of AA2014-T6 and AA7075-T6 alloys [13]

S. No.	Base material	Tensile strength (MPa)	Yield strength (MPa)	Elongation (%)	Hardness (HV)
1	AA2014-T6	452	383	7.5	75–85
2	AA7075-T6	487	417	11.5	105–115

Fig. 1 H13 steel tool used for the FSW process

Fig. 2 Experimental set-up of FSW machine

Experimental Set-up

During the FS Welding process, the tool rotational speed was varied from 540 to 1200 rpm at a constant welding speed. Based on workpiece material and thickness, the tool was selected. Variation of temperatures was measured using K-type Chromel-Alumel thermocouples. The thermocouples having the probe of diameter 1.5 mm was inserted into the hole, which was attached to the data logger. There was a high probability of damaging the thermocouples placed under the pin or tool shoulder. Therefore, the peak temperature was measured on the top surface of the workpiece slightly 2–3 mm away from the tool shoulder, as shown in Fig. 2. The tensile tests were performed on an Instron tensile testing machine using the ASTM E-8 standard specimens that were cut in the transverse direction. The crosshead velocity of the machine maintained at 1.5 mm/min and a strain rate of 0.0001 per second. Afterward, these specimens are polished over varying grit size papers over the welded zone. Eventually, the hardness was measured. Finally, the specimens were etched by the Keller's reagent mixture of HCl (3 mL), HF (2.0 mL), H_2O (190 mL) and HNO_3 (5.0 mL) for 20 s and then washed then with H_2O for 20 s.

Results and Discussion

The features of the weld depend on various parameters, i.e., welding speed, tool geometry, tool rotational speed, etc. Therefore, an optimum parameter is required for different alloys with different tool specifications. Table 5 summarized

the pattern of different tool rotational speeds. A large number of defects were identified for the joint produced at lower tool rotational speed. These defects may be due to the insufficient amount of material flow that results in void formation in Fig. 3. Similarly, at a higher tool rotational speed, the tunnel defect is found that is due to the lack of plasticized material available for the flow. The build-up formation of defects results in cracks (split of weldment), voids (unfilled scratch), improper mixing, wormhole, etc.

Variation of Temperature Profile

FSW has developed as a complicated and interdisciplinary process that requires a distinct set of knowledge and skills. Furthermore, the different physical and mechanical properties strongly depend upon the amount of heat generation, mechanical properties, mixing of materials, and material flow. Figure 4 depicts the response of temperature measurement by thermocouples at the tool rotation speed of 660 rpm. It has been found that the heating rate is more on the advancing side of the sheet as compared to the retreating side. Heating is due to the fact that the sheet has undergone severe plastic deformation that generates a large amount of

Table 4 H13 steel tool configuration [17]

S. No.	Tool variables	Dimension	
1	Depth of thread (mm)	0.5	
2	Pitch of thread (mm)	0.8	
3	Probe length (mm)	5.5	
4	Probe diameter (mm)	6	
5	Shoulder diameter (mm)	20	

Table 5 Summarized pattern of the dissimilar AA2014 and AA7075 alloys by FS welding process

Advancing side (AS)	Retreating side (RS)	Speed of tool rotation (rpm)	Welding speed (mm/min)	Remarks
AA 2014	AA 7075	540	30	Voids and cracks
AA 2014	AA 7075	660	30	Voids
AA 2014	AA 7075	840	30	Defect free
AA 2014	AA 7075	1020	30	Nugget collapse
AA 2014	AA 7075	1200	30	Tunnel defect
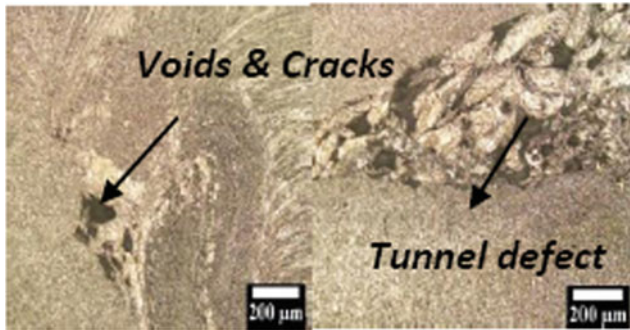
Fig. 3 Formation of defects in FS welding process by expanding tool rotational speed

heat. The peak temperatures were found to be around 309 °C on the AS while 264 °C on RS.

Although in Fig. 5 at 1200 rpm, the peak temperature reaches to 352 °C which is higher than the recrystallization temperature, i.e., 330 °C that predicts that the softening

region had been extended beyond the tool shoulder diameter at higher tool rotational speed [13]. Furthermore, an identical trend also observed in the temperature profile, which concluded that enhancing the tool rotational speeds results in increment in the amount of heat generation and vice versa.

Micro-hardness Analysis

For studying the mechanical properties, the hardness measurement has been carried out using the Vickers hardness machine by applying the force 200 gm with the dwell time of 20 s at room temperature. The average hardness values for alloys AA7075-T6 and AA2014-T6 were found to be 108 ± 0.2 HV and 77 ± 0.2 HV, respectively. This hardness Value is analogous to the earlier result reported by Saravanan [14]. Figure 6a depicts the hardness profile of Al-alloys for the dissimilar welding joint at a particular speed of tool rotation. Finally, the effect of hardness value within the stir zone is
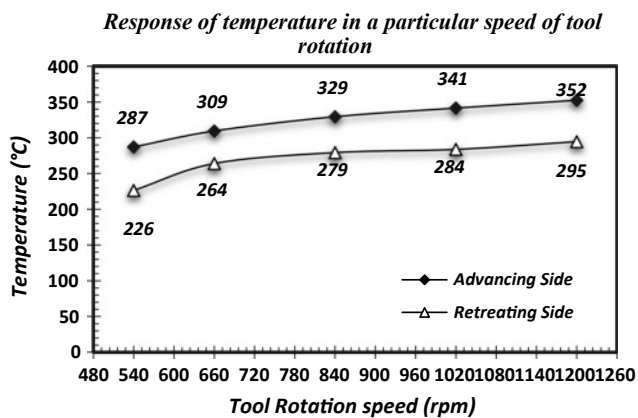
Fig. 4 Response of the temperature at the speed of tool rotation at 660 revolutions per minute

Response of temperature in a particular speed of tool rotation

Fig. 5 Response of temperature in a particular speed of tool rotation

lower in the RS region than AS. The figure provides the hardness values for all the regions available in the welded joint and the base metals. The mixing of materials determined the hardness in the welded region during the FS Welding process. The hardness value of HAZ is found to be lower than that of the base metals, but in SZ, the value is slightly higher. Increased values in both TMAZ and SZ lead to the change in plastic deformation and recrystallization that led to grain structure changes, as shown in Fig. 6b. With an increase in speed, extreme heat is generated, which dissolves the strengthening precipitates, and it coarsens the grains. However, in the nugget zone, the entire dissolution of precipitates occurs while coarsening the grain structure. Re-precipitation in the nugget zone of AA7075-T6 placed on the AS might have taken place upon natural aging and cooling, which are liable for this recovery in Hardness. Therefore, (Fig. 6) to acquire the proper amount of material mixing and grain coarsening for higher hardness value at a particular tool rotational speeds occurred in SZ due to plastic flow [15].

Tensile Strength Analysis

The tensile test specimens were taken from all the joints evaluated, and curves plotted in Fig. 7 for two alloys at different tool rotational speeds. In tensile test experiments, specimens were at room temperature with a crosshead velocity of 1.5 mm/min. The different parameters, including the ultimate tensile strength, yield strength, and percentage of elongation, were determined and reported in Tables 6 and 7. Both Tables show the parameters along with the efficiency of particular tool rotational speed. The deformation for the welded specimen in the transverse direction is highly heterogeneous, which is due to the microstructure that has different properties across the weld zone. Although with the constant welding speed, higher tool rotational speed resulted

in a heat input per unit length and stirring action, which affects the tensile strength. When the tool rotational speeds have come to the optimum speed, it generates sufficient heat input to the stir materials resulting in the proper material mixing and higher tensile strength [16]. Concerning the constant welding speed and tool geometry, the tensile strength increases with the increase in tool rotational speed and then drops with a further increase in the tool rotational speeds. At lower tool rotational speed, the amount of heat generated is low as the contact area is less, which is due to the insufficient material movement from the advancing side to the retreating side. Whereas at higher tool rotational speed, the amount of heat input is higher, which is due to the high heat input turbulence of material flow. The optimum results obtained at the proper inter-mixing of the material and grain coarsening, which is due to the plastic flow rate.

Microstructural Analysis

Microstructure analysis has been carried out along the welded cross-section of the sheet, which consists of three different zones, namely (a) Heat Affected Zone (b) Thermo-Mechanically Affected Zone (c) Nugget Zone as shown in Fig. 8. The microstructure analysis at the different zone is carried out at various tool rotation speeds. They are depicted in Figs. 9, 10, 11 and 12. It is observed that there is a recognizable variation of grain structures in various regions using Stereo Microscopy. It implies that the inter-mixing zone gradually enhances with the increase of tool rotational speed, but it has a greater influence than that of the welding speed.

Although, the Stir zone primarily contains fine recrystallized grains and obtained at the maximum temperature due to the strict plastic deformation. Adjacent to SZ (Stir Zone), TMAZ (Thermo-Mechanical Affected Zone) is found, which is defined by the existence of partially recrystallized grains as it is experienced lower heat input than SZ. HAZ (Heat Affected Zone) is found adjacent to the base metals, which experienced the only variation of temperature. Figure 8 shows the variation of the macro-structure of the specimen at various speeds of tool rotation, which is evidenced by the material flow behavior of the welding zone. The microstructure of the BM (Base Metal) of Al alloys is shown in Fig. 8. Although, occurs due to the variation of temperature in some cases, but it does not show any visible change either in its properties or microstructure.

In the case of the HAZ region structure of grains was elongated, which are analogous to the base metal (Fig. 10). The dynamic recrystallization is absent in this zone due to the deficiency of plastic deformation. Since the heat input at this region is low, there was no considerable change in the structure of the grains. The figure below depicts the same
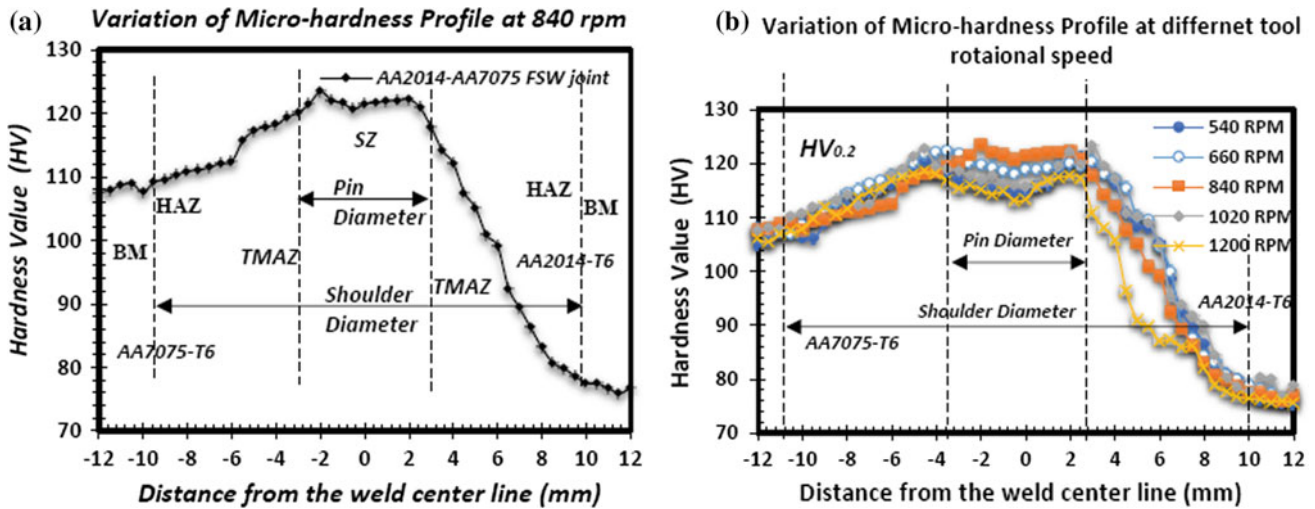
Fig. 6 Variation of micro-hardness profile: **a** at 840 revolutions per minute and **b** at different tool rotational speeds
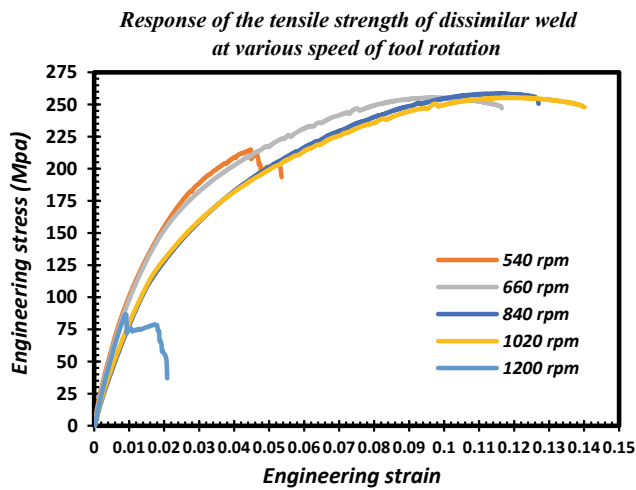

Fig. 7 Response of the tensile strength of dissimilar AA2014 and AA 7075 Al alloys at various speed of tool rotation

experimental conditions that can be seen while performing. In the HAZ region, the un-dissolvable strengthening precipitates combined together and formed large precipitates.

The microstructure of TMAZ consists of plastically deformed and a pattern of grain distortion in (Fig. 11). In the TMAZ region, the grains are bending forward in the direction of welding speed, i.e., at the AS, whereas it is in the opposite direction in RS. In the TMAZ region, grains are partly recrystallized and entire deformed regions. The scope of plastic deformation is not restricted in TMAZ. The strengthening precipitates might be dissolved in the TMAZ, as well.

While a special type of zone is found in certain materials or alloys that experienced the most severe deformation, which is known as "nugget zone or stir zone (SZ)" is shown in Fig. 12e. Formation of an onion ring-like structure is identified, which might be due to the deposition of the molten material having a threaded tool. Although an increase in tool rotational speeds enhances the enormous movement of material, which helped to achieve the higher heat generation. The coarsening of the fine recrystallized grain is found to be occurred due to the heat generation during the FSW process.

The second phase particles of Al–Cu–Mg–Zn were identified in the retreating side, which reflects that all the precipitates haven't dissolved in the material. SEM-EDS (Energy-Dispersive X-ray Spectroscopy) is evaluated, which represented in Fig. 13, that gives the existence of Al–Cu–Mg–Zn as the major constituents. The analysis is summarized in the table below along with their compositions. It might be observed that these precipitates influence the mechanical properties of the welded joints [14].

The corresponding grains which illustrated in Table 8 at different tool rotational speeds. Smaller grain size in the range of 4-6 microns is observed at a particular tool rotation

Table 6 Mechanical properties of dissimilar welds of AA2014 and AA7075 Al alloy at particular tool rotation speed of 840 revolutions per minute

Mechanical properties of Al. alloys at a particular speed of 840 rpm						
Yield stress (MPa)	Yield strain	Resilience (Pa)	UTS (MPa)	Ductility (%)	Elasticity (MPa)	Toughness (J/m^3)
113 ± 0.3	0.014 ± 0.001	0.88 ± 0.01	259 ± 0.4	13 ± 0.3	8455 ± 0.1	25 ± 0.1

Table 7 Mechanical properties of dissimilar welds AA2014 and AA7075 Al alloy at various tool rotational speeds

S. No.	Tool rotational speed (rpm)	Ultimate tensile strength (MPa) (±0.3)	Yield strength (MPa) (±0.4)	Elongation (%) (±0.1)	$\eta_{weld\ Joint}$ (±0.02)
1	540	215	102	5.5	47.5
2	660	255	108	11.6	56.5
3	840	259	113	13	57
4	1020	256	110	14	56.5
5	1200	151	93	5	32.5

Fig. 8 Dissimilar welded zone of the cross-section in tool rotational speed: **a** at 540 rpm; **b** at 840 rpm and **c** at 1200 rpm
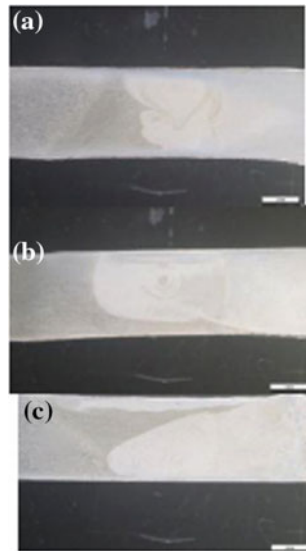
speed. Whereas, the fine equiaxed grains of 10 ± 0.2 μm observed due to severe plastic deformation. The grain growth happens due to the higher tool rotation; which leads to more heat generation. The grain growth takes place, as a side effect of higher heat generation of the particles of the precipitate dissolved in the base metal.

Fracture Analysis

In SEM (Scanning Electron Microscopy), images of the fractured surfaces at a particular tool rotational speed, which was joined using the FSW process, are shown in Fig. 14. Some FEG-SEM (Field Emission Gun Scanning Electron Microscopy) observations were taken to understand the microstructural effects on fractures surfaces of the specimens. The fractography clearly shows that it was covered
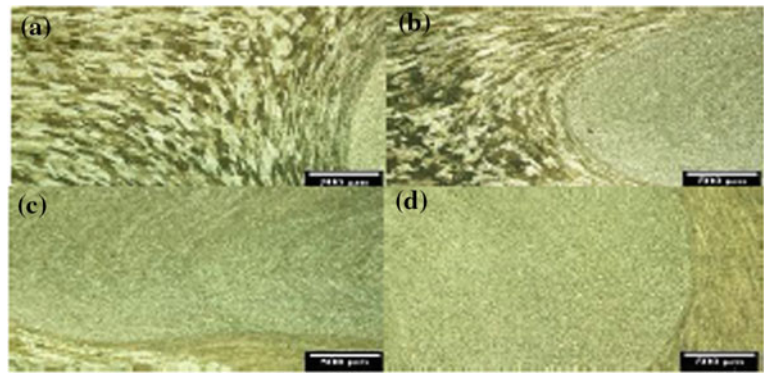
Fig. 9 Microstructure of (BM) base metal in various speeds of tool rotation for RS: **a** at 660 rpm; **b** at 840 rpm and for AS: **c** at 600 rpm; **d** at 840 rpm
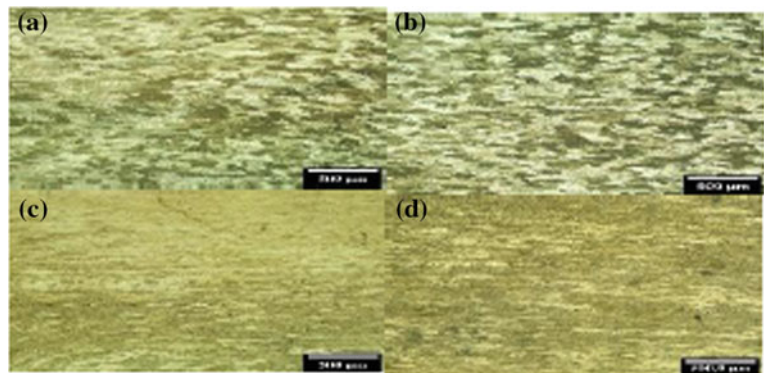

Fig. 10 Microstructure of HAZ in various speeds of tool rotation for RS: **a** at 660 rpm; **b** at 840 rpm and for advancing side: **c** at 600 rpm; **d** at 840 rpm
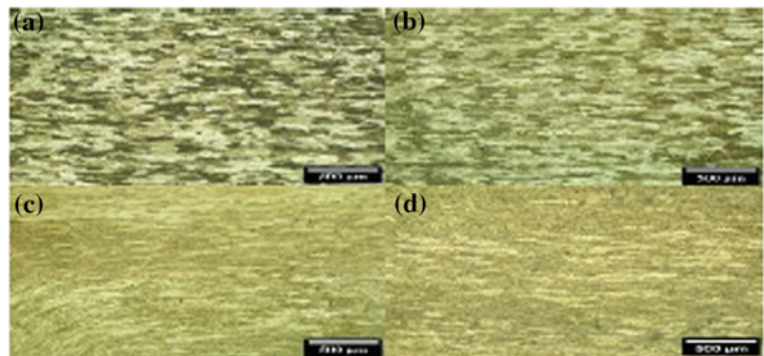
Fig. 11 Microstructure of TMAZ in various speeds of tool rotation for retreating side: **a** at 660 rpm; **b** at 840 rpm and for advancing side: **c** at 660 rpm; **d** at 840 rpm

Fig. 12 Microstructure of SZ in various speeds of tool rotation for retreating side: **a** at 660 rpm; **b** at 840 rpm, for advancing side: **c** at 660 rpm; **d** at 840 rpm and onion rings formation: **e** at 660 rpm; **f** at 840 rpm
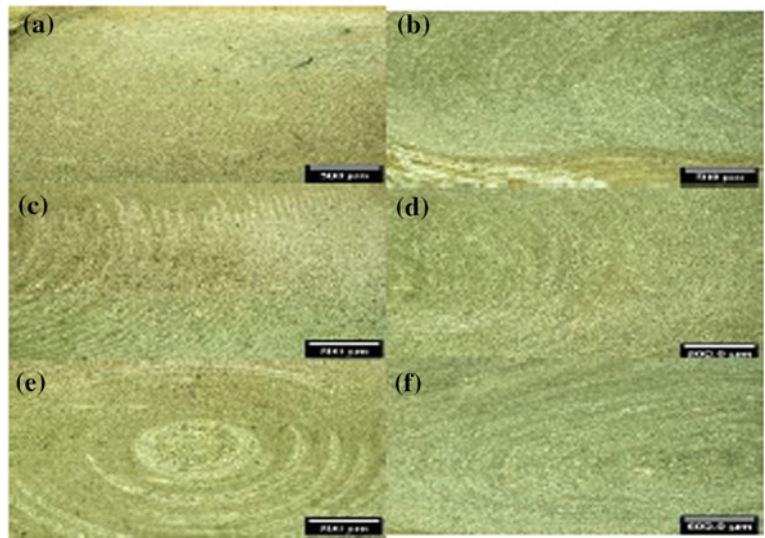
**Fig. 13** Elemental analysis of constituents using SEM analysis
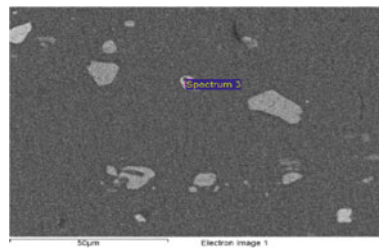
Element	Weight%	Atomic%
Mg K	1.14	1.81
Al K	44.67	64.19
Si K	1.20	1.65
Cu L	53.00	32.34

Table 8 Variation of rotational tool speed at different grain size within different zones

Tool rotational speed (rpm)	AA2014-T6		AA7075-T6				
	BM (±0.04)	HAZ (±0.03)	TMAZ (±0.0.1)	SZ (±0.01)	TMAZ (±0.01)	HAZ (±0.03)	BM (±0.04)
540	50	42.3	21.2	9.9	14.2	16.2	20.8
660	49	42.3	22.5	10.3	14.5	16.5	21.6
840	51.5	44	24.2	12.5	15.5	17	22.2
1020	52.4	45	25.7	12.7	15.7	17.4	22.3
1200	52.9	45.4	25.9	13	15.9	17.2	22.4
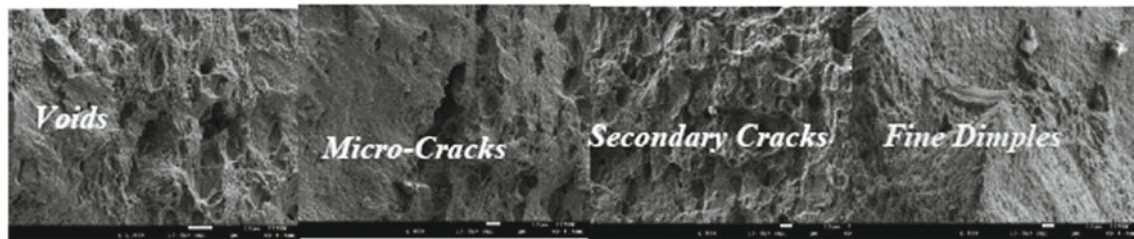
Fig. 14 Fractography of tensile specimens of welded joint in various speed of tool rotation

with fine dimples and a large population of micro-voids of different shapes and sizes. The failure of the joints was due to the propagation of these micro-voids during loading. The fractured position of the tensile specimens can also be predicted by fractography—fracture has taken place at different regions i.e., breaking at HAZ of RS or TMAZ of RS. Therefore, the tensile specimens fractured at the weakest point i.e., RS of the weld. Such a phenomenon is observed due to the low values of micro-hardness value found in the softer region.

Conclusion

In the present study, FS Welding of dissimilar plates AA2014-T6 and AA7075-T6 Al alloys of thickness 6 mm in a particular speed of tool rotation successfully performed. The following conclusions are driven based on the above results and discussions:

1. The max tensile strength of 258 ± 0.2 MPa with 113 ± 0.2 MPa yield strength and a maximum elongation of 12.7 (%) has found at a tool rotation speed of 840 rpm. Hence, 840 rpm is the optimum tool rotation speed.
2. Within the weld zone, the minimum hardness is observed in the HAZ region on RS, whereas the maximum hardness has been found in SZ, i.e., 122 ± 0.2 HV at 840 rpm due to the proper mixing of materials.
3. The microstructure of the SZ produced confirms the presence of fine recrystallized grain, which helps in obtaining the superior tensile strength and the micro-hardness of the joints.
4. As defects seem to occur during the intermixing zone at a higher speed of tool rotation. This phenomenon has improper mixing due to the enormous variation of microstructure in both the materials.
5. The micro-hardness value increases with an increase in tool rotation speed at RS, whereas it decreases on AS due to the coarsening of grains. The maximum grain size has been achieving in HAZ on both the AS and RS. While the maximum hardness achieved in SZ is due to the re-precipitation.

6. Using FEG-SEM analysis, all the joints were fractured mainly in HAZ or TMAZ on the RS leaving. The SZ is free from defects after the welding process. While, finest grain size is obtained at 540 rpm, i.e., 10 ± 0.2 μm.

References

1. W.M. Thomas, E.D. Nicholas, J.C. Needham, M.G. Murch, P. Templesmith, C.J. Dawes (1991) Friction stir welding. G.B. Patent Application No.9125978.8. December 1991
2. Murr L.E. (2010) A Review Research on dissimilar metal and alloys systems. J. of Materi Eng and Perform. 19:1071–89. https://doi.org/10.1007/s11665-010-9598-0
3. W.M. Thomas and E.D. Nicholas (1997) Friction stir welding for the transportation industries. Mat and Des. 18:269–273. https://doi.org/10.1016/s0261-3069(97)00062-9
4. W.M. Thomas, E.D. Nicholas, J.C. Needam, M.G. Murch, P. Templesmith, C.J. Dawes (1995) Friction Welding. US Patent No. 5460317. October 1995
5. K.V. Jata, K.K. Sankaran, J. Ruschau (2000) Friction stir welding effects on microstructure and fatigue of aluminium alloy 7050-T7451. Metall and Mat Trans A. 31:2181–2192. https://doi.org/10.1007/s11661-000-0136-9
6. J. Sinke, MM Stofregen, and E. Estraatsma, (2005) Tailor-made blanks for the aircraft industry: A Pilot Study, Technical report, Netherlands Institute for Metals Research, Netherlands
7. S. Rajakumar, C. Muralidharan, and V. balasubramanian, (2010) Optimization of the friction stir welding process and tool parameters to attain a maximum tensile strength of AA7075-T6 aluminium alloy. Proc. IMechE Part B J. Engg Manuf. 224:1175–1191. https://doi.org/10.1243/09544054jem1802
8. J.Q. Su, T.W. Nelson, R. Mishra and M. Mahoney (2003) Microstructural investigation of friction stir welded 7050-T651 aluminium. Acta Materialia. 51:713–729. https://doi.org/10.1016/s1359-6454(02)00449-4
9. C.G. Rhodes, M.W. Mahoney and W.H. Bingel, R.A. Spurling (1997) Effect of friction stir welding on microstructure of 7075

aluminium. Scripta Materialia. 36:69–75. https://doi.org/10.1016/s1359-6462(96)00344-2

10. P. L. Threadgill, A. J. Leonard, H. R. Shercliff and P. J. Withers (2009) Friction stir welding of aluminium alloys. Int. Mat Rev. 54:48–52. https://doi.org/10.1179/174328009x411136

11. W. M. Thomas, D. G. Staines, I. M. Norris, R. de Frias (2003) Friction stir welding Tools and developments. Weld Wor. 47:10–17 https://doi.org/10.1007/bf03266403

12. K. Colligan (1999) Material flow behaviour during friction stir welding of aluminium. Weld. J. Suppl. 78: 229 s–237 s

13. M.J. Jones, F.J. Humphreys (2002) Interaction of recrystallization and precipitation: The effect of Al3Sc on the recrystallization behaviour of deformed aluminium. Acta materialia. 51:2149–2159. https://doi.org/10.1016/s1359-6454(03)00002-8

14. V. Saravanan, Nilotpal Banerjee, R. Amuthakkannan and S. Rajakumar (2015) Microstructural evolution and mechanical properties of friction stir welded dissimilar AA2014-T6 and AA7075-T6 Aluminium alloys joints. Metallogr, microstruc and anal. https://doi.org/10.1007/s13632-015-0199-z

15. N. Pathak, K. Bandyopadhyay, M. Sarangi, S.Panda (2012) Micro-structure and mechanical performance of friction stir spot-welded aluminium-5754 Sheets. J. of Materi. Eng and Perform. 22:131–144. https://doi.org/10.1007/s11665-012-0244-x

16. K. Elangovan, V. Balasubramanian (2008) Influences of Tool Pin Profile and welding Speed on the formation of Friction Stir processing zone in AA2219 Aluminium Alloy. J. of Materi. Process. Technol. 200:163–175. https://doi.org/10.1016/j.jmatprotec.2007.09.019

17. R. Rai, A. De, H.K.D.H. Bhadeshia and T. DebRoy (2011) Review: friction stir welding tools. Sci & Tech. of Weld. and Join. 16:325–342. https://doi.org/10.1179/1362171811y.0000000023